Stokes wave over cavitating vortex

Eduard Amromin

Mechmath LLC, Edmond, Oklahoma, USA

Abstract

Following Stokes, several authors have studied waves with 120-degree angles at their crests caused on a free surface of fluid by the gravity force. Mathematical analysis, however, shown that similar Stokes waves can be caused by centrifugal force on surfaces where the pressure is constant, and cavitating tip vortex can be examined as a surface of an eventual appearance of axissymmetrical Stokes waves. Determination of shape of such vortices is a novel non-linear problem in potential theory. Thus, a special attention is paid to successive validation of intermediate computations. The main characteristics of the cavity-wave couples past a semi-ellipsoid are computed. An attempt to establish an association between the considered utmost steady flow and experimental data related to breakdown of cavitating vortices is done.

1. Introduction

This mathematical study was provoked by a recent experiment with cavitating tip-vortices. Usually a very large cavity stretches along the tip-vortex axis, and the cavity surface is smooth. However, this surface starts to be wavy in a quite narrow ranges of the vortex intensity and free-stream speed (Franc et al, 1995), and for a certain combination of the flow parameters, the cavity has been broken down by short parts that follow the vortex axis. Because the vortex induces an azimuth motion of fluid around the axis, it makes sense to examine the centrifugal force effect as an eventual cause of the wave appearance and to associate the cavity break with utmost steady conditions of existence of waves of maximum amplitude over the cavity. This way is promising because the highest gravitation-caused waves (observed either in Ocean, or in basins) are close to the computed Stokes waves (which are steady gravitation-caused waves of maximum amplitude). The observations at shoreline give $max\{Fr\}$~0.76, the solution for the Stokes waves in shallow water (by Amromin et al,1994) gave $max\{Fr\}$~0.79; here $Fr=U_\infty/(gH)^{0.5}$, H is the water depth, U_∞ is free-stream speed.

There are many publications on Stokes waves caused by the gravity force in 2-D flows (from Michell (1893) till Karabut (1998) papers) and in axissymmetric flow (Amromin, et al, 1990). These examinations were carried out in the framework of potential theory. The same way can be used here. There is, however, an essential innovation in the current analysis: a non-perturbed free boundary must be found here as a solution of another non-linear potential problem (in the case of gravity-generated waves, non-perturbed free surface is the plane y=0). This makes it necessarily to involve many successive validations.

Nomenclature

A=U_∞Ro/Γ - main dimensionless parameter of flow
C – free boundary
$Fr=U_\infty$/(gH) – Froude number
h(z) – distance between initial and corrected boundaries
H - water depth
L –cavity length
N – normal to the flow boundary
P – pressure
P_∞ - unperturbed pressure
q – density of φ
Ro – body radius
R – radial coordinate
r_{co}- corrected radius of free boundary
r_{in} - initial radius of free boundary
$r=R/Rcr$
Rcr – wave crest radius
S – flow boundary
U_∞- free stream speed
V – dimensionless velocity projection in meridian plan of flow
v – perturbation of V due to a boundary correction
Z – axial coordinate (abscissa)
Zo –abscissa of cavity detachment
Γ - intensity of vortex
$\sigma=2(P_\infty-P)/\rho U_\infty^2$ - cavitation number
$\sigma^*=2(Po-P)/\rho U_\infty^2$- modified cavitation number
ρ - fluid density
Φ - velocity potential
φ - auxiliary velocity potential

2. Mathematical formulation of problem

Let the fluid is ideal and incompressible, the flow is steady and curl-free. Consequently, the fluid velocity vector **U** can be defined as **U**=grad(Φ), where the velocity potential Φ is a solution of the Newman problem for the Laplace equation:

$$\Delta\Phi=0 \tag{1}$$

$$\partial\Phi/\partial N\big|_S=0 \tag{2}$$

$$\mathrm{grad}(\Phi)\big|_{z\to\pm\infty}=\{U_\infty,0,0\} \tag{3}$$

The problem (1)-(3) has a solely solution for any shape of the surface S. Contemporary custom CFD codes provide such solutions with a high accuracy. However, additionally to Eq.(2), the condition $P\big|_C=Constant$ has to be satisfied on a free boundary C that is a part of S, and, consequently, this condition predetermines the shape of S. In this problem, the pressure constancy condition can be written as

$$(\Gamma/2\pi R)^2+|U|^2+2P/\rho=C_1=Constant$$

Here Γ/2πR is the azimuth component of velocity, and U is velocity projection on meridian section of flow. The conventional cavitation number σ is composed with the non-perturbed pressure, but introduction of an auxiliary constant $Po=\rho\,(C_1-U_\infty^2)/2$ and modified cavitation number σ^* allows operations with a simpler form of the Bernoulli equation.

A flow sketch is given in Fig.1. The Riabushinsky mirror-scheme (Birkhoff & Zarantonelo, 1957; Brennen, 1969) is selected here. The wave looks turned out, but one has to keep in mind that these Stokes waves are caused by centrifugal force. The acute crest has the smallest radius $R=Rcr$. If the fluid rotation starts at the cavity detachment section $z=Zo$ where the body has the radius Ro, then $C_1=U_\infty^2+2P_\infty/\rho+(\Gamma/2\pi Ro)^2$. Such a jump of the azimuth velocity takes place past a marine propeller, for example. Because the mirror-scheme is used, the opposite jump of the azimuth component of velocity exists also at $z=-Zo$.

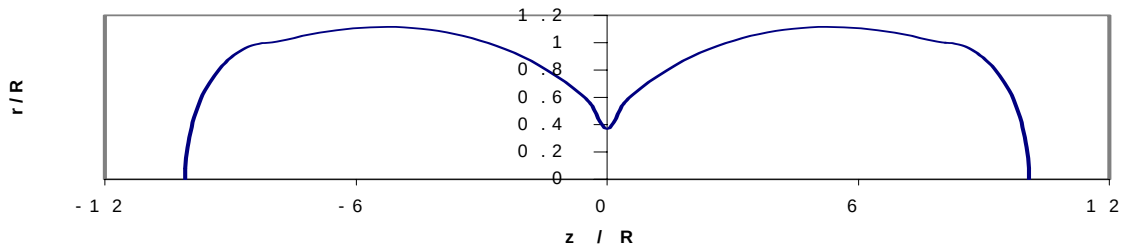

Figure 1: Meridian section of Stokes solitary wave over axissymmetric cavity. The symmetric Riabushinsky scheme is used for cavity modeling. The section has curvature jumps at the points of free surface joints to the body (here at z/R=±8.08).

One can rewrite the pressure constancy condition as $(\Gamma/2\pi RU_\infty)^2+V^2=1+\sigma^*$, where $\sigma=\sigma^*-(1+\sigma^*)(Rcr/Ro)^2$ $V=U/U_\infty$. Consequently, σ^* and Γ are not independent, and $\Gamma/(2\pi U_\infty Rcr)=(1+\sigma^*)^{1/2}$. Using the ordinate Rcr as the length unit, one can transform the pressure constancy condition to the following equation:

$$[\mathrm{grad}(\Phi)/U_\infty]^2=(1+\sigma^*)(1-1/r^2) \tag{4}$$

Here the dimensionless velocity V manifestly depends on the function $r(z)$ and the solely constant σ^*. Cavitation number σ here becomes a hidden parameter that can be found after solving the non-linear problem (1)-(4) only, because the ratio Rcr/Ro has to be known for calculation of σ.

Thus, the solutions of Eqs.(1)-(4) depend on the only auxiliary parameter σ*, and this problem looks similar to the traditional problems of ideal cavitation.

3. Method to solve nonlinear problem

An iterative perturbation method (Amromin et al, 1994) was used to solve this non-linear potential problem. For a selected shape of C (obtained from the previous iteration or initially given), the solution of the Newman problem (1)-(3) gives a $V(z)$ distribution over S (including the current approach to C). Such a distribution generally

will not satisfy to Eq.(4). Substitution of the *V(z)* into Eq.(4) allows determination of a difference between the desirable and actual distribution of the velocity along the free surface. If this difference is denoted as *v(z)* and $|v(z)|<<1$, one can deduce the following formula for *v(z)* from Eq.(4):

$$2v = [(1+\sigma^*)(1-1/r^2)]^{1/2} - V^2/[(1+\sigma^*)(1-1/r^2)]^{1/2} \qquad (5)$$

It is necessary to modify the *C* shape to obtain the velocity variations that shall satisfy to Eq.(5). Let *C** is a desirable modification of *C*, and $|h/L|<<1$, $|\partial h/\partial s|<<1$, where *s* is tangent to *C*. An auxiliary velocity potential φ can be introduced: $v=grad(\varphi)$. Taking into account Eq.(2) on *C*, one can deduce the following linear condition on *C** for φ:

$$\partial\varphi/\partial N+\partial(hV)/\partial s = 0 \qquad (6)$$

Further, Eq. (5) can be rewritten as the linear equation:

$$\frac{1}{\pi}\int_0^{s(L)}\frac{q(\xi)}{s-\xi}d\xi = \frac{N_r}{r^2-1}\left[\frac{\gamma\sqrt{r^2-1}}{V(s)r^2}+\frac{V(s)}{\gamma\sqrt{r^2-1}}\right]\int_0^s q(\xi)d\xi + \gamma\sqrt{1-1/r^2} - \frac{rV^2(s)}{\gamma\sqrt{r^2-1}} \qquad (7)$$

Here N_R is the radial component of *N*. The pair of the linear equations (6), (7) allows determination of the function *h(z)* when functions $\{V(z),\ \gamma(z)=[1+\sigma^*][r^2(z)-1]\}$ are known after solving Eqs.(1)-(3). If φ is a potential of the sources of an unknown density *q(z)*, this density should be small, but the equation (7) is then a singular integral equation with the Cauchy core, and the function *q(z)* can be limited only when an additional condition takes place:

$$[1+\sigma^*]\int_0^{s(L)}\sqrt{\frac{[1-r(s)^{-2}]}{[s(L)-s]s}}ds = \int_0^{s(L)}\frac{V^2(s)ds}{\sqrt{[s(L)-s][1-r(s)^{-2}]s}} \qquad (8)$$

According to Gakhov (1966), $q(0)=q(L)=0$ when Eq (8) is satisfied; otherwise *q* rise up to the infinity at least at one of the above points. Fortunately, this condition gives the only pair $\{L,\ \sigma^*\}$ that allows a permanent free boundary correction (avoiding breaks of N in iterations). For the hydrodynamic problem in the whole, it allows determination of cavitation number for a given length of the free boundary.

The equations (6)-(8) are used for the iterative corrections of the free boundary. Each iteration starts from solving the problem (1)-(3) out of the corrected *S* and computation of *V*. Because this linear problem can be solved within a high accuracy, the right hand of Eq.(5) can be also well-computed. So, when the right hand of Eq.(5) becomes small enough in all points of *C*, this surface shape is close enough to the solution of the whole nonlinear problem (1)-(4), and the iterations can be finished. The most important singularities of these iterations have to be emphasized.

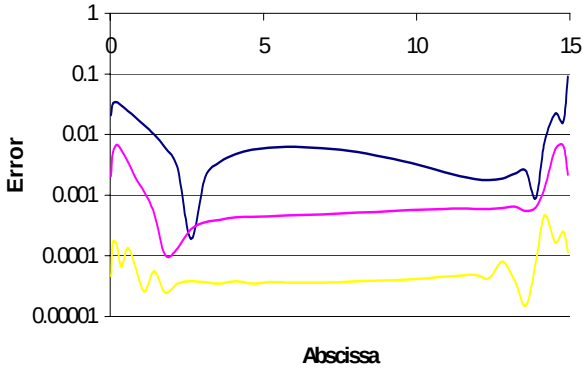

Figure 2. Error distributions along the free boundary. Upper curve corresponds to iteration number 10, median curve to iteration number 30, down curve to 90th iteration

First of all, for the selected kind of φ, the equation (6) is the first-order differential equation relatively *h*, and this equation has to be solved with the condition *h(0)=0*. Nevertheless, the condition *h(Zo)=0* also has to be satisfied, because the boundary must be continue at *z=Zo*. Therefore, its radius will be corrected under the rule

$$r_{co}(z)=r_{in}(z)+h(z)N_R(z)-h(Zo)N_R(Zo),$$

and the ratio of the body radius *R* to *Rcr* will be found as a result of such corrections.

Secondly, in any iteration, the 120 degrees-angle at the crest has to be fixed: this angle cannot appear in the solution as a result of continue transforms.

Thirdly, denominators in several terms in Eq.s.(7),(8) drop to zero near the crest, and an employment of an asymptotic expansion in the crest vicinity has to be matched with the numerical solution of Eqs.(6)-(8).

A typical error drop during the above-described computation is shown in Fig. 2. There are at least five sources of errors in numerical solving such a non-linear problem. First, consideration of an area with continuous boundaries must be replaced by examination of equations and boundary conditions in a limited number of points. Second, integrals have to be replaced by sums, as well as derivations have to be replaced by finite differences. Third, because the problem is non-linear, iterations have to be used. Fourth, the unknown values must be really found from a linear algebraic system that really replaces both integral and differential equations. Fifth, any computer operates with a limited number of decimal places. A complete analysis of all mentioned errors never was done in a paper on fluid mechanics. Thus, one can consider the above manifestation of 6 decimal places as something questionable. Nevertheless, such a table illustrates the iteration convergence.

4. Intermediate results: axissymmetric ideal cavitation

A much more informative validation of nonlinear solution can be done by comparison of the intermediate results with previously validated solutions of appropriate problems. As such a validation, there are comparisons with data related to the axissymmetric cavities in flows without azimuth components of velocity ($V^2=1+\sigma$ on *C*). The comparison in Fig.3 relates to cavities past disk computed by Brennen (1969). There is no exact analytical solution for axissymmetric cavitating flows, and such a comparison is the only accessible mathematical validation.

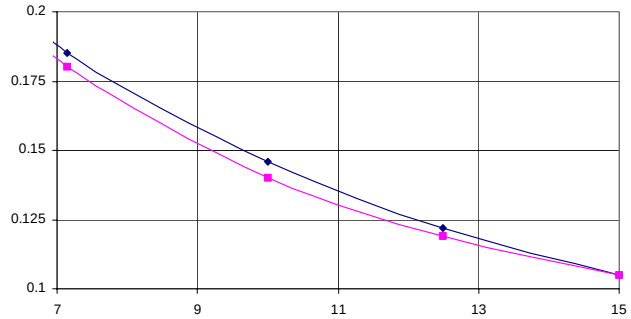

Figure 3: Computed cavity length past disk versus cavitation number. Presented result (top) is compared with the Brennen's result (bottom).

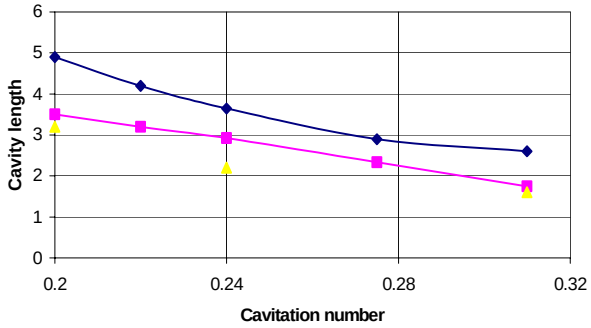

Figure 4: Cavity length for ellipsoid of revolution $z^2/4+r^2=1$. ▲ - observation by Ivanov (1980), ■ - computation with cavity detachment located in observed points; ♦ - computation for cavity detachment determined with the Brilluin-Villa condition.

There is also comparison of measured and computed cavity length of an ellipsoid (in Fig.4) that will be employed in the following computations in this paper. The computed drag coefficient for diverse ellipsoids is compared with coefficients measured by Ceitlin (1960) and Epstein (1961) in Fig.5. Their drag was measured in a basin, and their diameters were 0.05m.

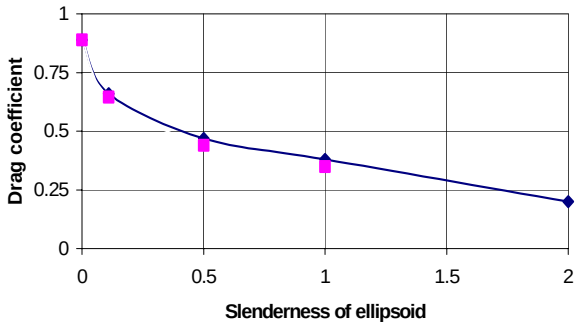

Figure 5: Drag coefficient of ellipsoids of revolution versus their slenderness at σ=0.1. Computed results are shown by solid curve, ■ - experimental data.

5. Intermediate results: gravity-caused Stokes waves

Determination of gravity-caused waves is mathematically similar to the considered problem. For gravity-caused waves, $2yFr^{-2}+V^2=1$ on C, and the velocity also directly depends on the free surface ordinate. The described numerical technique to determine Stokes waves was earlier (Amromin, et al, 1994) validated by comparison with the classical result by Michell (1983), and the practical coincidence was obtained for this flow. The infinite systems of the 2-D Stokes waves in shallow water were then considered, and one can see in Fig.6 the *Fr* effect on their wavelength.

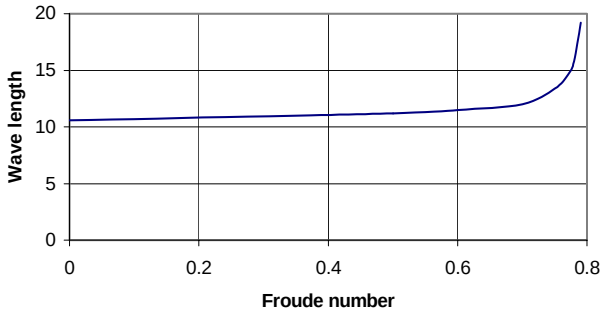

Figure 6: Effect of Froude number *Fr* on the Stokes wavelength in shallow water ($Fr=U_\infty/(gH)^{1/2}$, H is the depth).

The next comparison relates to the solutions of two different (but very close) problems: the shape of the Stokes wave of maximum length in shallow water (Amromin et al, 1994) was compared with the Stokes solitary wave (Guzevski,1982) in Fig.7. There is a practical coincidence in the used scale; the crest ordinate, however, was 1.815 for periodical waves (later Korabut (1998) gave 1.827) and 1.832 for solitary wave (by Guzevsky(1982); later Longuet-Higgins & Fox(1996) gave 1.833).

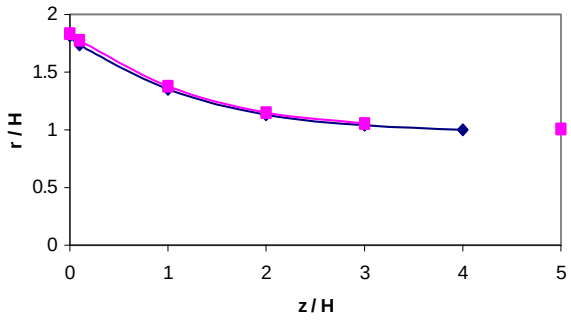

Figure 7: Shapes of the largest Stokes waves. ♦ -computation by Amromin et al; ■ - by Guzevski.

6. Numerical results for centrifugal Stokes waves

The rotation-caused Stokes waves are currently examined for the only body. This body is the semi-ellipsoid of revolution $z^2/4+r^2=1$. The cavity detachment is fixed at the section $z= Zo$. As noted, the only Stokes wave can exist for a given value of cavitation number, and the relevant σ value is coupled with Γ. Thus, the parameter $A=U_\infty R/\Gamma$ is selected as the solely parameter for the presentation of the numerical results. Comparing gravitation-caused and centrifugal Stokes waves, one can find similar roles of *Fr* and *A*. As a result, the dependency of the wavelength *L* on *A* in Fig.8 is similar to *L (Fr)* in Fig. 6: there is also a sharp rise of *L* at a maximum value of a governing parameter. This value is *A*=0.5634 for centrifugal Stokes waves past this semi-ellipsoid.

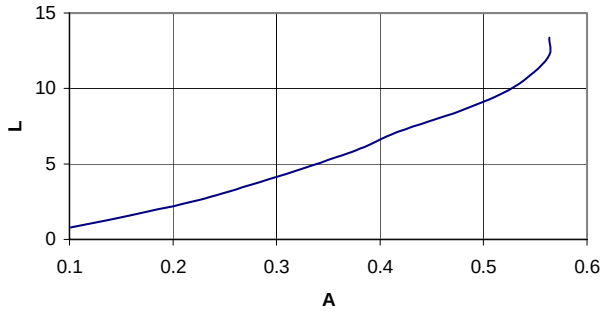

Figure 8: Length of centrifugal Stokes waves as function of the parameter $A=U_\infty R/\Gamma$

The wave amplitude can be calculated as the difference between the maximum radius of free boundary and its minimum radius that equals to *Rcr*. These extreme radiuses are plotted in Fig.9. Comparing Figs.8 and 9, one can find that the generation of centrifugal Stokes waves (centrifugal steady maximum-amplitude waves) requires higher Γ for shorter free surfaces.

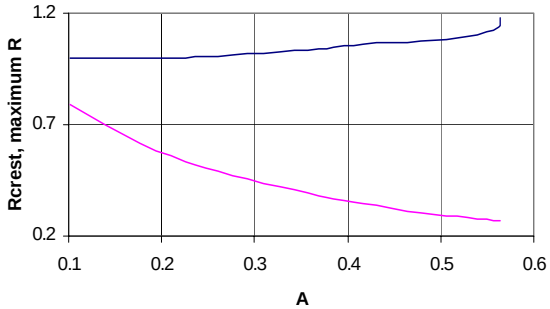

Figure 9: Maximum radius B of free boundary (top curve) and its minimum radius *Rcr* (bottom curve) versus A.

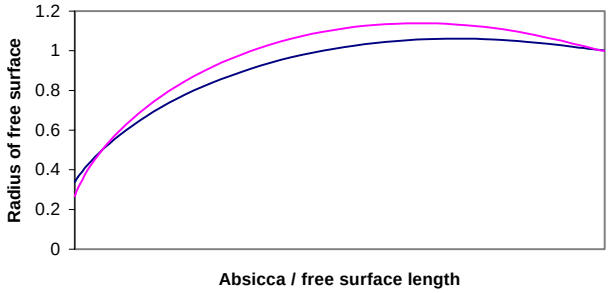

Figure 10: Typical meridian sections of cavitating vortices with the centrifugal Stokes waves. The wavelengths are reduced to the same scale.

The typical meridian sections of a half cavity are shown in Figure 10. The longitudinal scales are reduced here to have a possibility to compare the centrifugal force effect on the free surface shape. A larger cavity is wider in the whole, except of a relatively small region near the crest.

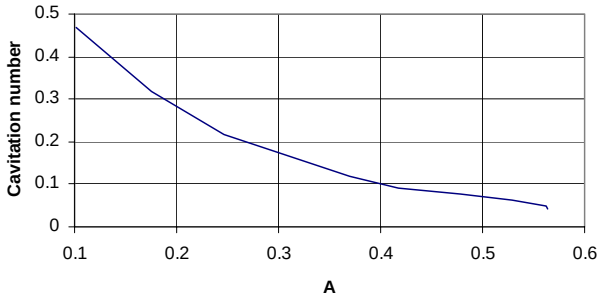

Figure 11: Minimal cavitation number for a cavitating vortex as function of A=U_∞R/Γ

Remembering the above-mentioned mutual dependency of σ and Γ in this problem, it is interesting to find the cavitation number as a function of A. This function is shown in Fig.11. The minimum of attainable σ values is 0.041. It is evident that such a minimum must be positive because of a contribution of the azimuth velocity to the fluid momentum.

There are some data in experiments with cavity breakdown in vortices (see Franc et al, 1995, and Castro et al, 1997), but the above papers do not give the sufficient information for a direct comparison of computed results with observed waves. Nevertheless, it seems, the mentioned situation with two kind of vortex cavitation can be clarified by these computations. The cavitation types should be branched when the couple $\{\Gamma,\sigma\}$ is suitable to Stokes waves. For a smaller Γ, the wave crest radius has to be larger; for a higher Γ, the cavity will be broken, like wavebreaking occurs with the gravitation-caused waves in shallow water.

7. Conclusions

The presented Figures give the sufficient information about the exact numerical solutions of the nonlinear mathematical problem (1)-(4). These solutions are quite complete from mathematical point of view and well validated by successive comparison of intermediate data with appropriate known numerical solutions. The satisfactory convergence of iteration is also manifested. The obtained utmost steady solution can be employed to an analysis of breakdown of cavitating vortices.

Acknowledgment

The author thanks Professor D.H. Peregrine for the useful discussion.

References

Amromin,E.L., Basin, M.A.. & Bushkovsky,V.A. (1990) “Two solution of the three-dimensional problem of limiting waves on the surface of a heavy fluid”. Appl. Math. Mech., Pergamon ,v54, pp162-166

Amromin,E.L., Ivanov,A.N. & Sadovnikov,D.Yu. (1994) “Bottom effect on limited Stokes waves”, Fluid Dynamics, v29, pp540-543
Birkhoff,G & Zarantonelo,E. (1957) “Jets, Wakes and Cavities” Ac. Press.
Brennen,C.E. (1969) “A numerical solution for axisymmetric cavity flows”. JFM,v37, pp671-688
Castro,F., Crespo,A., Manuel,F. & Fruman,D.H. (1997) “Equilibrium of Ventilated Cavities in Tip Vortices”, Journ. Fluids Eng., v119, pp759-767
Ceitlin, M.Y. (1960) “Drag of cavitated ellipsoids of revolution”, Trudy TAGI, v801, pp1-20 (in Russian)
Epshtein, L.A. (1961) “Flow past bodies of revolution at small cavitation numbers”, Trudy TAGI, v817, pp1-14 (in Russian)
Franc,,J.-P., et al. (1995) “La cavitation”. Presses Universitaires de Grenoble (in French).
Gakhov, F.D. (1966) “Boundary Value Problems”, Pergamon
Guzevski,L.G. (1982)“Flow of heavy fluid of finite depth past obstacles “ in: *Continium Dynamics*, Cheboksary (in Russian)
Ivanov, A.N. (1980) “Hydrodynamic of Cavitating Flow”, Leningrad, Sudostroenie (in Russian)
Karabut, E.A. (1998) “An approximation for the highest gravity waves on water of finite depth”, JFM, v372, pp45-70
Longuet-Higgins,M.S. & Fox,M.J.H. (1996) “Asymptotic theory for the almost-highest solitary wave”, JFM, v317, pp1-19
Michell,J.H. (1893) “The highest wave in water”, Phil. Magazine, ser.5, p430